Crystallization of Isotactic Polypropylene from Prequenched Mesomorphic Phase

Takashi Konishi, Koji Nishida,* and Toshiji Kanaya

Institute for Chemical Research, Kyoto University, Uji, Kyoto-fu 611-0011, Japan

Received January 26, 2006; Revised Manuscript Received July 25, 2006

ABSTRACT: The crystallization process of isotactic polypropylene (iPP) by heating from the prequenched mesomorphic phase has been studied using wide-angle X-ray diffraction, small-angle X-ray scattering, and optical microscopy. Mesomorphic iPP as quenched shows the well-known nodular structure of ca. 100 Å. In heating process the nodules grew larger keeping self-similarity, with the mesomorphic phase partially transforming into the crystalline phase inside the nodules. After reaching the isothermal process, the nodules stopped to grow at a certain quasi-equilibrium size depending on the annealing temperature. During the long annealing, the interface among the nodules became obscure, and the nodules in nanometer scale merge into larger structure of pure α-phase in micrometer scale. The relation between the quasi-equilibrium nodule size and the annealing temperature leads an extrapolated melting temperature of the mesomorphic phase, which is located above the equilibrium melting temperature of the α-crystal.

1. Introduction

Isotactic polypropylene (iPP) has three kinds of polymorphism for crystalline structure (α-, β-, and γ-form)[1−4] and intermediate state between amorphous and crystal, the so-called "mesomorphic phase".[5,6] The crystalline structures are specified by four types of 3/1 helices (the combination of left- and right-handed helices and up and down stems concerning the CH_3 group).[4] The mesomorphic phase also consists of 3/1 helices; however, the sense of helix (left- and right-handed) has no particular rule.[7] The mesomorphic phase of iPP is obtained when molten iPP is quenched fast enough to prevent outbreak of crystallization. Such a condition is achieved by quenching below 0 °C at a rate faster than 80 °C/s.[8] The structure of mesomorhpic phase has been explained as smectic phase[5,6] or crystal having some defects.[9−13] In our previous paper,[14] we found that the formation mechanism of the mesomorphic phase of iPP is quite analogous to that of lyotropic liquid crystal.[15−21] In the formation process of the mesomorphic phase of iPP, helical segments of iPP played roles as mesogens of liquid crystal as was also pointed out by Li and de Jeu.[22−24] The morphology of the mesomorphic iPP in nanoscopic scale is characterized by the so-called "nodule" of polygonal or spherical shape as was observed by transmission electron microscope (TEM).[6,25,26] The diameter of the nodule is ca. 100 Å at room temperature. The internodular distance confirmed by small-angle X-ray scattering (SAXS) measurement roughly corresponds to the diameter of the nodule observed by TEM.[6] The mesomorphic phase is transformed into α-form crystalline phase in keeping nodular morphology when the mesomorphic iPP is heated above 40 °C.[27] However, the mechanism of the transformation is not sufficiently understood. To clarify it, we have examined the crystallization process from the mesomorphic phase using wide-angle X-ray diffraction (WAXD), SAXS, and optical microscopy (OM).

Recently, Strobl proposed a model of polymer crystallization via intermediate state between amorphous and crystal.[28] According to the model, granular domains of mesomorphic phase are formed first in the induction period of the crystallization, next mesomorphic phase is transformed into crystalline phase in the granular domains, and finally the crystalline granular domains merge into lamellar structure. The model also predicts that equilibrium melting temperature of the mesomorphic phase is located at a higher temperature than that of crystalline phase. We will discuss analogy and difference between the crystallization model with the present crystallization from the prequenched mesomorphic phase.

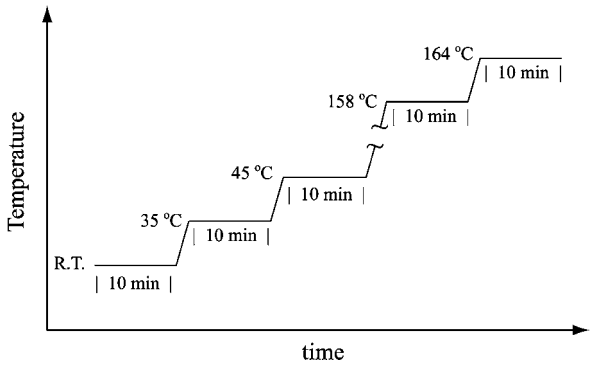

Figure 1. Temperature protocol for the WAXD measurements.

2. Experimental Section

2.1. Materials and Sample Preparations. The iPP material has a weight-average molecular weight $M_w = 208\,000$ and a polydispersity of $M_w/M_n = 5.47$, which was supplied from Mitsui Chemical Co. Ltd. A degree of isotacticity (a meso pentad value) of the iPP determined by ^{13}C NMR was 0.982. A mesomoprhic phase thin film was obtained by quenching from the molten state to 0 °C dipping into ice−water. For SAXS and WAXD measurements, the sample films 200 μm thick were plied 5-fold to ensure the scattering intensity. Sample films 20 μm thick sandwiched between cover glasses were used for optical microscopic observation.

2.2. WAXD Measurements. The WAXD measurements were carried out using a Rigaku Denki R-AXIS IV diffractometer with ultraX 18 (18 kW) X-ray generator. A Mettler FP82HT hot stage was used for the temperature control of samples. The temperature was raised stepwise, holding 10 min at each temperature for the measurement (Figure 1). The measurements were conducted at room temperature, 35, 45, 55, 75, 90, 105, 120, 140, 155, 158, and 164 °C.

* Corresponding author: e-mail knishida@scl.kyoto-u.ac.jp; tel +81-774-38-3141; fax +81-774-38-3146.

10.1021/ma060191b CCC: $33.50
Published on Web 10/18/2006

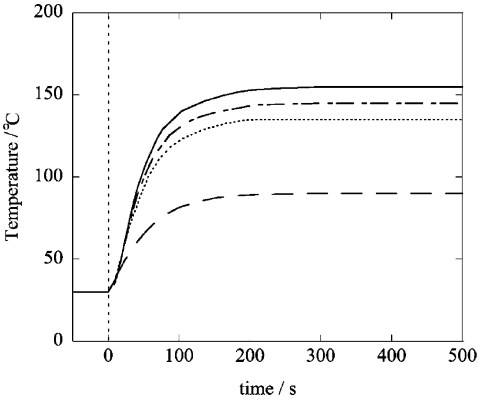

Figure 2. Thermal histories of iPP samples annealed at 90 (broken line), 135 (dotted line), 145 (chain line), and 155 °C (solid line) for time-resolved SAXS measurements.

2.3. SAXS Measurements. The SAXS measurements were carried out using the beamline BL-10C in Photon Factory at High Energy Accelerator Research Organization, Tsukuba, Japan. The SAXS covered a range of scattering vector q ($= 4\pi \sin\theta/\lambda$; λ and 2θ being X-ray wavelength and scattering angle, respectively) from 6.0×10^{-3} to 1.8×10^{-1} Å^{-1}. Using a two-heat-capacitors-type temperature controller, samples were heated from room temperature to the annealing temperatures 50−158 °C. Figure 2 shows examples of thermal histories of the samples when heated to 90, 135, 145, and 155 °C in this temperature controller. The samples reached the prescribed temperatures within ca. 200 s. The time-resolved SAXS measurements were conducted throughout the heating process (<200 s) and the subsequent isothermal process (>200 s).

2.4. Optical Microscopic Observation. The time evolution of the optical micrographs was recorded with a Nikon Optiphot2-Pol with a charge coupled device (CCD) camera and a video recorder. The temperature controller for optical microscopic observation was a laboratory-made apparatus, which is commercially available from Japan Hightech and Linkam as LK-300. This temperature controller is able to heat up and down very rapidly (≫80 °C/s).[29,30]

3. Results and Discussion

3.1. Component Analysis in Heated Mesomorphic iPP. First, we surveyed the change in fractions of the mesomorphic, α-crystal, and amorphous phase when the mesomorhic iPP was heated from room temperature to 164 °C in the manner prescribed in Experimental Section. Parts a, b, and c of Figure 3 show examples of in-situ WAXD profiles at room temperature, 90, and 155 °C, respectively. For each WAXD profile component analysis was carried out assuming each profile consist of α-crystal, mesomorphic, and amorphous fractions. α-crystalline Bragg peaks appear at $2\theta = 14.1°$, 16.9°, 18.6°, 21.6°, and 21.9°.[5,10] The Bragg peaks of mesomorphic phase appears at $2\theta = 15°$ and 21°.[5,10] An amorphous halo of iPP appears at $2\theta = 17°$. It should be noted that γ-crystalline Bragg peaks which usually appear in the normal crystallization from melt[31−33] were hardly observed in this crystallization. Fitting curves and their constituents are also displayed in Figure 3. The WAXD profile of the mesomorphic iPP at room temperature has two characteristic broad peaks (Figure 3a). The fraction of the mesomorphic iPP was 52%, and the rest is amorphous. At 90 °C the α-crystalline Bragg peaks appear, but the two mesomorphic peaks still remain (Figure 3b). The fractions of the mesomorphic phase, α-crystal, and amorphous were 26%, 26%, and 48%, respectively, at 90 °C. At 155 °C the α-crystalline peaks increase further in intensity (Figure 3c). The fraction of the mesomorphic phase could not be detected at 155 °C anymore. The fractions of the α-crystal and amorphous were 40% and 60%, respectively, at 155 °C. Thus, the fractions of mesomorphic phase,

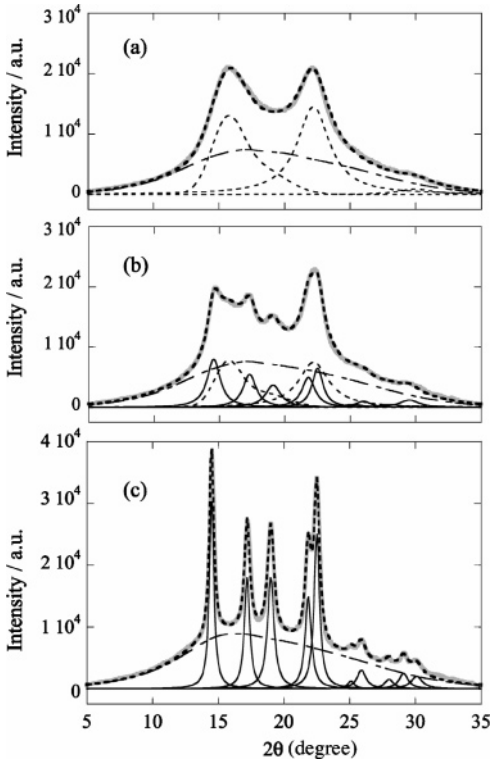

Figure 3. WAXD profiles of the mesomorphic iPP at room temperature (a) and the mesomorphic iPP heated to 90 °C (b) and 155 °C (c). Observed (thick gray lines) and fitting (thick dotted lines) curve reproduced by summing up the constituents separated by the component analysis where α-crystalline form (thin solid lines), mesomorphic phase (thin dotted lines), and amorphous phase (thin chain lines).

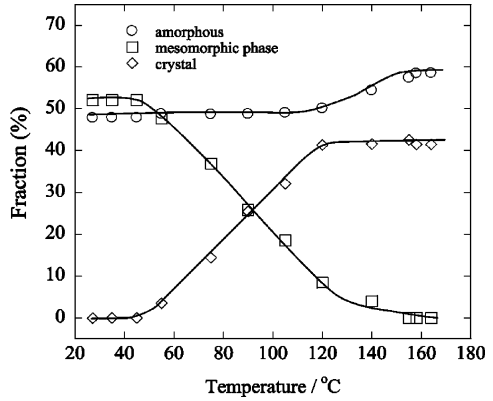

Figure 4. Temperature dependence of fractions of amorphous, crystal, and mesomorphic phase during stepwise annealing as shown in Figure 1.

amorphous, and crystal were obtained for each prescribed temperature (Figure 4).

The fractions of the mesomorphic phase, amorphous, and crystal do not change below 45 °C. Wang et al. showed that the mesomorphic phase transforms into α-crystal above ca. 80 °C when the mesomorphic iPP is heated at a heating rate of 4 °C/min.[34] Martorana et al. pointed out that the mesomorphic phase is slightly transformed into α-crystal when the mesomorphic iPP annealed at 40 °C for a long time.[27] In the present condition, i.e., stepwise annealing with 10 min intervals, the transition from the meosomorphic phase into the α-crystal is observed above 45 °C. It should also be noted that the mesomorphic iPP is highly transformable[35] within the framework of the mesomorphic phase below such a meso-α transition temperature. Between 45 and 120 °C, the fraction of the crystal

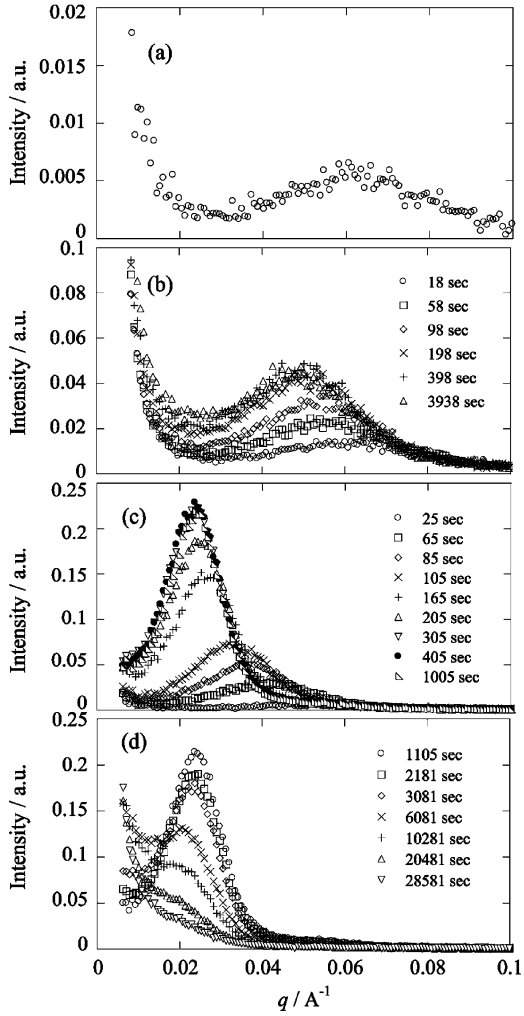

Figure 5. SAXS profile of mesomorphic iPP at room temperature (a) and time-resolved SAXS profiles of mesomorphic iPP when heated to 90 °C (b) and 155 °C before 1000 s (c) and after 1000 s (d).

increases with the annealing temperature, coinciding with decrease in the fraction of the mesomorphic phase. On the other hand, the fraction of the amorphous does not change below 120 °C. This behavior suggests that the mesomorphic phase only transforms into the α-crystal, and the amorphous is invariable between 45 and 120 °C. Above 120 °C, the α-crystal no more increases in the present annealing condition. The remaining mesomorphic phase starts to melt above 120 °C and completely melts into amorphous or molten state above 140 °C.

3.2. Evolution of Nodular Structure. Figure 5a shows a SAXS profile of the mesomorphic iPP at room temperature. The SAXS curve of mesomorphic iPP at room temperature has a weak peak at around $q_{max} = 0.065$ Å^{-1}. In general, it is difficult to determine whether the structure in question is nodular or lamellar only by the SAXS peak. However, as was evidenced by transmission electron microscopy (TEM),[6,25] both the fresh (room temperature) and annealed (155 °C for 4 h) mesomorphic phase show not the stacked lamellar but the nodular structure. Therefore, the q_{max} in the SAXS profile is attributable to the nodular structure. The details of the SAXS profile will be discussed in section 3.3.

Parts b and c of Figure 5 show time-resolved SAXS profiles for the mesomorphic iPP when heated to 90 and 155 °C from room temperature, respectively. As was noted in Experimental Section, the time periods before and after 200 s are heating process and isothermal process, respectively. When mesomorphic iPP was heated to 90 °C, the q_{max} shifted to lower side and the intensity I_{max} increased until 200 s (Figure 5b). After 200 s, i.e., in isothermal process, the SAXS profile was almost unchanged. When the mesomorphic iPP was heated to 155 °C, the q_{max} also shifted to lower side and the I_{max} increased in the heating process (Figure 5c). The variation of the SAXS profile gradually slowed down in early stage of isothermal process (<300 s). During a long period between 300 and 1000 s, the SAXS profile was almost unchanged. After showing such constancy, the I_{max} gradually decreased and the intensity in lower q region increased (Figure 5d).

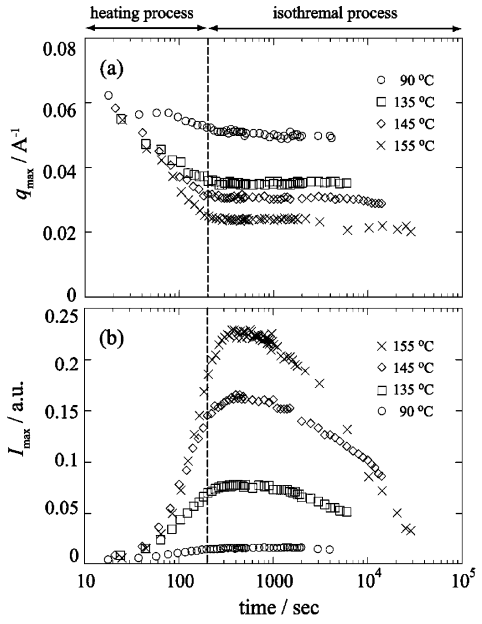

Figure 6. Time evolutions of q_{max} (a) and I_{max} (b) extracted form SAXS profiles of mesomorphic iPP annealed at indicated temperatures.

Figure 6a,b shows time evolutions of the q_{max} and I_{max} in the SAXS profiles when the mesomorphic iPP was heated to 90, 135, 145, and 155 °C. In the heating process (<200 s), all the q_{max}s shifted to lower side and all the I_{max}s increased. After 200 s the q_{max}s are almost invariable, but the I_{max}s still increased during the period between 200 and 300 s. During the period between 300 and 1000 s, all the q_{max} and all the I_{max}s remained the same. This characteristic behavior suggests the existence of a quasi-equilibrium state for the relation between the nodule size and annealing temperature. After ca. 1000 s, all the I_{max}s started to decrease. This behavior is more conspicuous at the higher temperatures and further accelerated after ca. 5000 s at 155 °C. Finally (>30 000 s, at 155 °C), the SAXS peak completely disappeared.

These SAXS results are interpreted as follows. In the heating process (<200 s), both the size of nodules and crystallinity inside the nodule increase. In early stage of isothermal process (<300 s), the size of nodular structure does not change, but within the nodules crystallization still proceeds. During the quasi-equilibrium state, apparent changes in size and quality of the nodular structure are not observed by SAXS, but some hidden rearrangement probably proceeds. In the late stage (>1000 s), the interface among the nodules becomes obscure, and the nodules merge into some larger structure. However, the merging of nodules should be very slow or not complete at low temperatures, considering that the data point of I_{max} at 155 °C and that of 145 °C cross each other around 10^4 s.

3.3. Self-Similarity in Nodular Structure. Figure 7 shows the SAXS profiles in logarithmic scales normalized by the q_{max} and I_{max} for the data already shown in Figure 5c. These

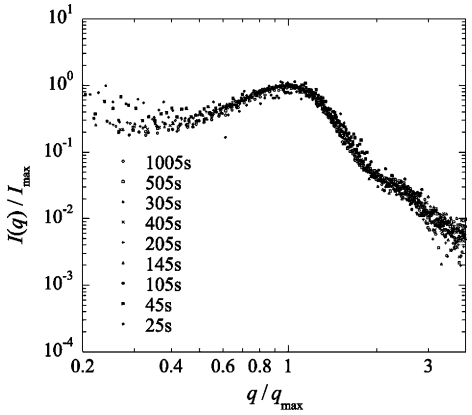

Figure 7. SAXS profiles of mesomorphic iPP annealed at 155 °C until 1000 s normalized by q_{max} and I_{max}.

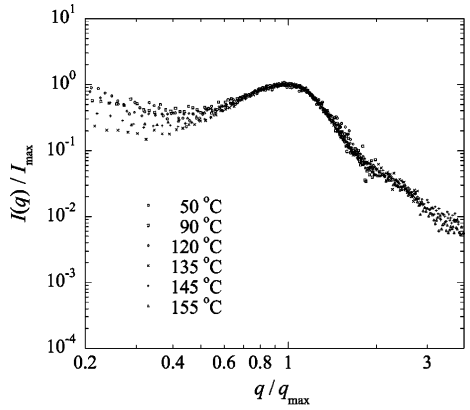

Figure 8. SAXS profiles of mesomorphic iPP annealed at different temperatures for 600 s normalized by q_{max} and I_{max}.

normalized profiles give a unique master curve except for the low region ($q/q_{max} < 0.5$). This interesting scaling is valid throughout the heating process and the quasi-equilibrium state (<1000 s). It should be noted that the master curve well reproduces a shoulder peak at around $q/q_{max} = 2.5$ besides the main peak at $q/q_{max} = 1.0$.

In general, the scattering function for a system of dispersed particles is described by a product of the structure factor and the form factor. The peak due to the structure factor usually appears in the lower q range than the peaks due to the form factor.[36] In a system of loosely packed spheres, the ratio of the q value of the first peak due to the form factor to that of the structure factor approximates 2.5.[37] The nodular structure shown by TEM[6,25] is very analogous to a system of loosely packed spheres. Therefore, the first peak and shoulder peak in Figure 7 are assigned to the structure factor and the form factor, respectively. Furthermore, as long as the ratio of q value of the former peak to that of the latter peak is kept constant, it can be said that the "self-similarity" in a relation between the outer size of nodules and their packing manner is kept.

The SAXS profiles of different temperatures at 600 s, i.e., the data in the quasi-equilibrium state, are collected in Figure 8 normalized by the q_{max} and I_{max}. These normalized profiles also give a unique master curve except for the low q region. Thus, the self-similarity is also kept for the different annealing temperatures.

3.4. Extrapolated Melting Temperature of Mesomorphic Phase. The relation between crystalline lamellar thickness l and melting temperature T_m is often discussed using the following Gibbs−Thomson equation:[38]

$$l^{-1} = \Delta H_m(T_m^\infty - T_m)/2\sigma_e T_m^\infty \quad (1)$$

where ΔH_m, T_m^∞, and σ_e are heat of fusion, equilibrium melting temperature of crystal, and specific energy of chain-folded surface, respectively. The lamellar thickness l is also related to the crystallization temperature T_c. Experimental[39−41] and simulation results[42,43] are well described by the following relation:

$$l^{-1} \sim (T_m^\infty - T_c) \quad (2)$$

Here, we will apply this relation to the case of nodule size ($\sim 1/q_{max}$), instead of the lamellar thickness l, as follows:

$$q_{max,e} \sim (T_m^\infty - T_a) \quad (3)$$

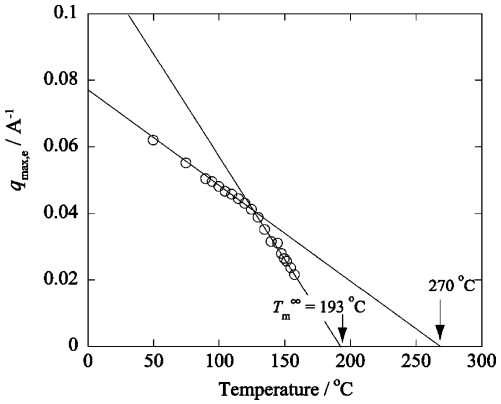

Figure 9. Temperature dependence of $q_{max,e}$ obtained from SAXS results for the mesomorphic iPP annealed at different temperatures.

where $q_{max,e}$ and T_a are the value of the q_{max} obtained in the quasi-equilibrium state and the annealing temperatures, respectively.

Figure 9 shows the $q_{max,e}$s vs the annealing temperatures T_a. Two straight lines can be drawn by fitting the data to eq 3. The crossover temperature of two lines is found at ca. 125 °C, which corresponds to a temperature where the remaining mesomorphic phase starts to melt as was revealed by the analysis of WAXD (Figure 4). One straight line drawn by fitting the data in the higher temperature region is extrapolated to 193 °C, which well corresponds to the value of the equilibrium melting temperature T_m^∞ of iPP crystal reported by Iijima and Strobl.[39] Another straight line drawn by fitting the data in the lower temperature region is extrapolated to ca. 270 °C. The melting temperature of mesomorpic phase in effect should be the above-mentioned crossover temperature. Therefore, the possibility of the mesomorpic phase above the crossover temperature is conditional, and the latter extrapolated temperature is considered hypothetical.

Formation mechanisms of the mesomorphic phase will afford a clue to this issue. The driving force of the mesomorpic phase formation is similar to that of liquid crystal, namly the parallel ordering of rodlike segments.[14,22−24] In the case of the mesomorpic phase of iPP, helical segments act as the rodlike segments. Therefore, stabilization of helical segments is essential to the mesomorphic phase. The lower the temperature is, the more the helical segments are stabilized.[44] There must be a temperature above which the helical segments are not stable enough to maintain the mesomorphic phase.

In the case of intrinsically rigid polymers, the equilibrium smectic−isotropic transition temperature T_i^∞ is located at higher

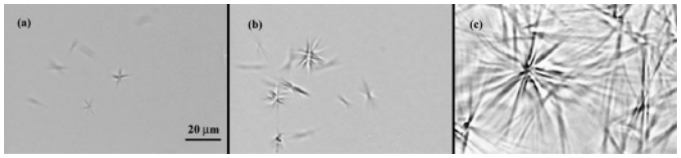

Figure 10. Optical micrographs of mesomorphic iPP annealed at 155 °C for 4.5 (a), 8 (b), and 26 h (c). A black bar represents 20 μm.

enough than the melting temperature of crystal phase, as was shown by Tokita et al.[45,46] Whereas, the mesomorphic phase of intrinsically flexible polymer should exist in limitted conditions. Kawai and Kimura reported that molten iPP chains could be oriented under magnetic field up to 240 °C.[47] Li and de Jeu found a shear-induced smectic phase of molten iPP at 215 °C.[22−24] It is noteworthy that these intermediate structures were observed at temperatures higher enough the equilibrium melting temperature of iPP crystal. Even in the quiescent state, the mesomorphic phase should last or exist as a superheating state under a brief exposure to the higher temperature than 125 °C. In fact, short time heating of the mesomorphic phase at 162 °C, much higher than 125 °C, significantly affected the subsequent crystallization at 130 °C.[30]

There are some discussions favorable to the high-temperature mesomorphic phase. Grebowicz et al. estimated the latent heat from mesomorphic phase to crystal to be ca. 0.6 kJ/mol.[11] Comparing this value to the melting heat of crystal 148 kJ/mol, the difference between the heat of fusion of the smectic (mesomorphic) and that of the crystal is negligible small. Li and de Jeu showed that the thickness of smecitic phase (mesomorphic phase) is larger than that of crystal when each annealing temperature was the same, while the surface energy of smectic phase should be smaller than that of the crystal.[24] These discussion leads that the smecitc phase has a higher melting temperature than the crystal's. The crystallization model via mesophase proposed by Strobl[28] is also predicting the existence of a higher melting temperature for the mesophase than the normal equilibrium melting temperature of crystal. Although his model intends originally to describe the crystallization mechanism from the molten state, it accounts for the high equilibrium melting temperature of the prequenched mesomorphic phase. In any case, trace of the mesomorphic phase will never remain above the hypothetical extrapolated temperature.

3.5. Morphology in Optical Microscopic Scale. Parts a, b, and c of Figure 10 show optical micrographs at 4.5, 8, and 26 h, respectively, when the mesomorphic iPP was rapidly heated to 155 °C. Any morphology in optical microscopic scale was not observed during the first 2 h. At 4.5 h, needlelike crystallites were observed (Figure 10a). The crystallites grew in size with annealing time (Figure 10b,c). It should be noted that no visible entity was observed within at least 8 h when the same iPP was crystallized at 155 °C directly from the melt. Nucleation of cryatallites is usually sporadic, but the shortening of the induction time when crystallized from the mesomorphic phase at 155 °C seems significant enough, although we have not yet compared the growth rate of the meso-crystallization with that of the melt-crysatallization at 155 °C.

On the other hand, these characteristic crystallites of micrometer size could not be observed at least within a day when crystallized from the mesomorphic phase below 140 °C. It can be said that the formation of morphology in micrometer scale is inhibited when crystallized from the mesomorphic phase below 140 °C, considering that large shperulites are easily obtained in a short period of time when the same iPP is crystallized directly from the melt below 140 °C. It is probably because that preformed nodules cannot or are very slow to merge into larger structure at low temperatures, as was discussed in section 3.2. Similar slowdown in crystallization behavior was reported for the crystallization from molten β-phase by Li et al.[48] In this case, the reason for the slowdown was explained that the preformed regular arrangement of right- and left-handed helices favorable to β-phase makes their rearrangement difficult.

Another characteristic of the needlelike crystallite, or the crystallization from the prequenched mesomorphic iPP, is a single-crystal-like nature. The needlelike crystallite does not show the long period, as was evidenced by the disappearance of SAXS peak. Namely, every needlelike crystallite does not consist of stacked lamellae. This point is a great difference from the crystallization model via the mesomorphic phase directly from the molten state, since the model proposed by Strobl[28] depicts that the nodules merge into the lamellar structure. As was noted in the result of WAXD, γ-phase free crystal was preferentially obtained by the crystallization from the prequenched mesomorphic iPP. Probably, the heating process from prequenched mesomorphic phase is more favorable to this characteristic behavior than the cooling process from melt, since the ratio of γ-phase to α-phase becomes smaller in the lower crystallization temperature.[31−33] The high purity of the α-phase should contribute to the single-crystal-like nature.[30]

Acknowledgment. We thank Prof. Kataoka, Nara Institute of Science and Technology, for the use of WAXD instrument. We also thank Dr. Fujio, Mitsui Chemical Co. Ltd., for the use of temperature controller for SAXS measurements.

References and Notes

(1) Natta, G.; Corradini, P. *Nuovo Cimento (Suppl.)* **1960**, *15*, 40.
(2) Mancik, Z. *J. Macromol. Sci., Phys.* **1972**, *36*, 101.
(3) Turner-Jones, A.; Cobbold, A. J. M. *J. Polym. Sci.* **1968**, *6*, 539.
(4) Lotz, B.; Wittmann, J. C.; Lovinger, A. J. *Polymer* **1996**, *37*, 4979.
(5) Natta, G. *SPE. J.* **1959**, *15*, 373.
(6) Hsu, C. C.; Geil, P. H.; Miyaji, H.; Asai, K. *J. Polym. Sci., Part B: Polym. Phys.* **1986**, *24*, 2379.
(7) Lotz, B. *Eur. Phys. J. E* **2000**, *3*, 185.
(8) Coccorullo, I.; Pantani, R.; Titomanlio, G. *Polymer* **2003**, *44*, 307.
(9) Hoseman, R.; Wilke, W. *Makromol. Chem.* **1968**, *118*, 230.
(10) Miller, R. *Polymer* **1960**, *1*, 135.
(11) Grebowicz, J.; Lau, S. F.; Wunderlich, B. *J. Polym. Sci., Polym. Symp.* **1984**, *71*, 19.
(12) Caldas, V.; Brown, G. R.; Nohr, R. S.; Macdonald, J. G.; Raboin, L. E. *Polymer* **1994**, *35*, 899.
(13) Ferrero, A.; Ferracini, E.; Mazzavillani, A.; Malta, V. *J. Macromol. Sci., Phys.* **2000**, *B39*, 109.
(14) Konishi, T.; Nishida, K.; Kanaya, T.; Kaji, K. *Macromolecules* **2005**, *38*, 8749.
(15) Doi, M.; Edwards, S. F. *The Theory of Polymer Dynamics*; Oxford: New York, 1986.
(16) Imai, M.; Mori, K.; Mizukami, T.; Kaji, K.; Kanaya, T. *Polymer* **1992**, *33*, 4451.
(17) Imai, M.; Mori, K.; Mizukami, T.; Kaji, K.; Kanaya, T. *Polymer* **1992**, *33*, 4457.
(18) Imai, M.; Kaji, K.; Kanaya, T. *Phys. Rev. Lett.* **1993**, *71*, 4162.
(19) Imai, M.; Kaji, K.; Kanaya, T. *Macromolecules* **1994**, *27*, 7103.
(20) Imai, M.; Kaji, K.; Kanaya, T.; Sakai, Y. *Phys. Rev. B* **1995**, *52*, 12696.
(21) Matsuba, G.; Kaji, K.; Nishida, K.; Kanaya, T.; Imai, M. *Macromolecules* **1999**, *32*, 8932.
(22) Li, L. B.; de Jeu, W. H. *Macromolecules* **2004**, *37*, 5646.
(23) Li, L. B.; de Jeu, W. H. *Phys. Rev. Lett.* **2004**, *92*, 075506.
(24) Li, L. B.; de Jeu, W. H. *Faraday Discuss.* **2005**, *128*, 299.

(25) Ogawa, T.; Miyaji, H.; Asai, K. *J. Phys. Soc. Jpn.* **1985**, *54*, 3668.
(26) Grubb, D. T.; Yoon, D. Y. *Polym. Commun.* **1986**, *27*, 84.
(27) Martorana, A.; Piccarolo, S.; Sapoundjieva, D. *Macromol. Chem. Phys.* **1999**, *200*, 531.
(28) Strobl, G. *Eur. Phys. J. E* **2000**, *3*, 165.
(29) Nishida, K.; Kaji, K.; Kanaya, T.; Matsuba, G.; Konishi, T. *J. Polym. Sci., Part B: Polym. Phys.* **2004**, *42*, 1817.
(30) Nishida, K.; Konishi, T.; Kanaya, T.; Kaji, K. *Polymer* **2004**, *45*, 1433.
(31) Alamo, R. G.; Kim, M. H.; Galante, M. J.; Isasi, J. R.; Mandelkern, L. *Macromolecules* **1999**, *32*, 4050.
(32) van der Burgt, F.; Rastogi, S.; Chadwick, J. C.; Rieger, B. *J. Macromol. Sci., Phys.* **2002**, *B41*, 1091.
(33) Nozaki, K.; Endo, Y.; Yamamoto, T.; Naiki, M. *J. Macromol. Sci., Phys.* **2003**, B42, 697.
(34) Wang, Z. G.; Hsiao, B. S.; Srinivas, S.; Brown, G. M.; Tsou, A. H.; Cheng, S. Z. D.; Stein, R. S. *Polymer* **2001**, *42*, 7561.
(35) Miyamoto, Y.; Fukao, K.; Yoshida, T.; Tsurutani, N.; Miyaji, H. *J. Phys. Soc. Jpn.* **2000**, *69*, 1735.
(36) Hashimoto, T.; Fujimura, M.; Kawai, H. *Macromolecules* **1980**, *13*, 1660.
(37) Kinning, D. J.; Thomas, E. L. *Macromolecules* **1984**, *17*, 1712.
(38) Strobl, G. *The Physics of Polymer*; Springer-Verlag: Berlin, 1997.
(39) Iijima, M.; Strobl, G. *Macromolecules* **2000**, *33*, 5204.
(40) Janimak, J. J.; Cheng, S. Z. D.; Giusti, P. A.; Hsieh, E. T. *Macromolecules* **1991**, *24*, 2253.
(41) Hauser, G.; Schmidtke, J.; Strobl, G. *Macromolecules* **1998**, *31*, 6250.
(42) Meyer, H.; Muller-Plathe, F. *J. Chem. Phys.* **2001**, *115*, 7807.
(43) Reith, D.; Meyer, H.; Muller-Plathe, F. *Macromolecules* **2001**, *34*, 2335.
(44) Antoniadis, S. J.; Samara, C. T.; Theodorou, D. N. *Macromolecules* **1999**, *32*, 8635.
(45) Tokita, M.; Osada, K.; Yamada, M.; Watanabe, J. *Macromolecules* **1998**, *31*, 8590.
(46) Tokita, M.; Osada, K.; Tsuchiya, H.; Watanabe, J. *Kobunshi Ronbunshu* **1999**, *56*, 184.
(47) Kawai, T.; Kimura, T. *Macromolecules* **2000**, *33*, 8421.
(48) Zhou, J. J.; Li, L.; Lu, J. *Polymer* **2006**, *47*, 261.

MA060191B